# Discovery of pyrazolopyrimidine derivatives as novel inhibitors of ataxia telangiectasia and rad3 related protein (ATR)

Sreekanth A. Ramachandran [a], Pradeep S. Jadhavar [a], Manvendra P. Singh [a], Ankesh Sharma [a], Gaurav N. Bagle [a], Kevin P. Quinn [b], Po-yin Wong [b], Andrew A. Protter [b,c], Roopa Rai [b], Son M. Pham [b,*], Jeffrey N. Lindquist [b,*]

[a] Integral BioSciences, Pvt. Ltd., C-64, Hosiery Complex Phase II Extension, Noida, Uttar Pradesh, 201306, India
[b] Medivation, Now Pfizer Inc., 525 Market Street, 36th Floor, San Francisco, CA 94105, United States
[c] Current address: Palo Alto Pharmaceutical Consulting Service, United States

ABSTRACT

The ATR pathway is a critical mediator of the replication stress response in cells. In aberrantly proliferating cancer cells, this pathway can help maintain sufficient genomic integrity for cancer cell progression. Herein we describe the discovery of **19**, a pyrazolopyrimidine-containing inhibitor of ATR via a strategic repurposing of compounds targeting PI3K.

© 2017 Elsevier Ltd. All rights reserved.

Damage to cellular DNA, from intrinsic and extrinsic sources, are dealt with constantly in normal human cells. The DNA-Damage Response (DDR) is a complex process that has mechanisms specifically tailored for the type of DNA damage encountered.[1,2] These mechanisms may involve activation of checkpoint response, cell-cycle arrest, and DNA-repair or apoptosis in response to DNA-damage. In normal, healthy cells this response results in either a correction of the damage, or, if the damage is too extensive to repair, leads to cell death via apoptosis. In cells with oncogenic transformation, the DNA-damage response may be upregulated to enable rapid division and deal with the increased replicative stress of the enhanced rate of cell division.[3–6] The approval of olaparib (formerly AZD2281)[7] by the US FDA in 2014 for the treatment of certain forms of advanced ovarian cancer demonstrated the clinical benefit of inhibiting one component of the DDR pathway namely poly(ADP-ribose) polymerase (PARP).[8–10]

Another critical component of the replication stress response is the ataxia telangiectasia and rad-3 related protein (ATR), a member of the phosphatidylinositol 3-kinase-related protein kinase (PIKK) family.[11–13] This family also includes the DNA-damage response proteins, ataxia telangiectasia mutated (ATM) and DNA-dependent protein kinase (DNA-PK).[14] Together all three proteins maintain genomic surveillance and stability in proliferating cells. ATR is the primary responder to replication stress in cells, including replication stress due to treatment with DNA-damaging agents like gemcitabine and hydroxyurea.[15] In this scenario, ATR activates checkpoint response and regulates the transition of S-phase to G2-phase to allow time for DNA repair and reducing efficacy of DNA-damaging agents. In addition, in cells lacking proper p53 activity, and thus a proper regulation of G1 to S-phase, are more dependent upon ATR pathway for survival and proliferation. This makes ATR an attractive target to increase tumor sensitivity to DNA-damaging agents,[16,17] combine with other agents targeting DNA-Damage-Repair, such as PARP inhibitors,[18] or as a monotherapy in certain indications/genotypes.[19]

Recent reports have described utilizing homology between ATR and phosphoinositide 3-kinase (PI3K) as a means for guiding ATR inhibitor design.[20–23] Our labs have recently reported the discovery of small-molecule Bruton's tyrosine kinase (BTK) and PI3Kδ dual inhibitors and we sought to employ this collection to identify inhibitors of ATR.[24] Towards this end, we selected compounds from our library of BTK and PI3Kδ dual inhibitors and screened them against ATR at 0.5 and 5 μM (Eurofins Scientific, Dundee, Scotland). The results from this initial screen are graphically illustrated in Fig. 1.

Among the 299 compounds tested, 11 compounds inhibited ATR activity to >50% at 5 μM whereas at 0.5 μM only 1 compound inhibited ATR activity to >50%. Surprisingly, an analysis of ATR and

* Corresponding author.
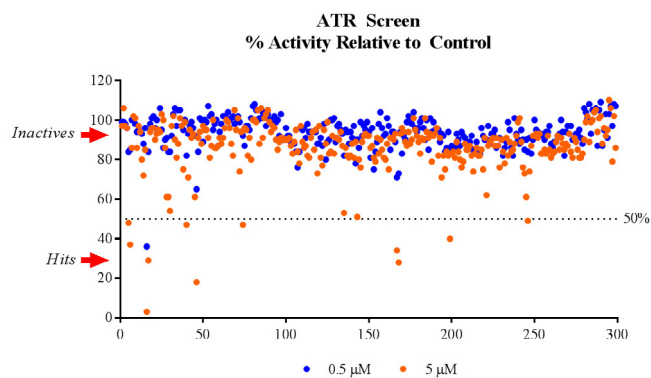  *E-mail address:* pham.sm@gmail.com (J.N. Lindquist).
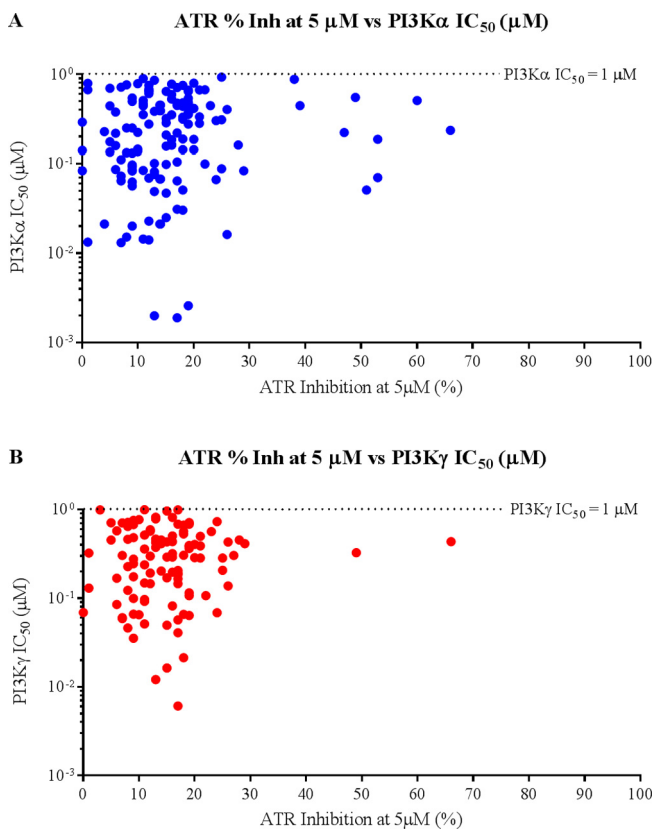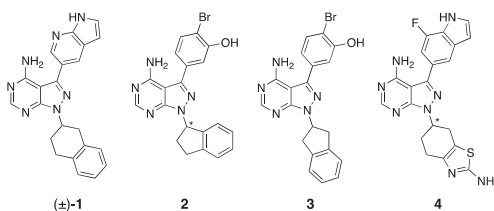
**ATR Screen**
**% Activity Relative to Control**



**Fig. 1.** ATR percent activity at 0.5 and 5 µM.

**A**   **ATR % Inh at 5 µM vs PI3Kα IC$_{50}$ (µM)**



**B**   **ATR % Inh at 5 µM vs PI3Kγ IC$_{50}$ (µM)**



**Fig. 2. A.** ATR % inhibition vs PI3 Kα IC$_{50}$; **B.** ATR % inhibition vs PI3 Kγ IC$_{50}$.

**Table 1**
Hits from ATR screen.



| Compound[a] | ATR IC$_{50}$ (µM) | ATR LipE | BTK IC$_{50}$ (µM) | PI3 Kδ IC$_{50}$ (µM) |
|---|---|---|---|---|
| (±)-**1** | 0.212 | 3.2 | ND[b] | ND[b] |
| **2** | 1.86 | 1.5 | 0.123 | 0.155 |
| **3** | 3.56 | 1.4 | 0.012 | 0.010 |
| **4** | 2.63 | 2.6 | 0.022 | 0.307 |

[a] Compound **1** is racemic.
[b] ND, IC$_{50}$ not determined.

PI3Kα/γ inhibition showed relatively poor correlation of inhibitory activity between these protein targets, Fig. 2. These results suggested that using PI3K homology to guide optimizations would not be feasible with this chemical series. Therefore we would likely need to construct single-point changes in order to identify the key binding interactions on ATR as part of a larger effort to improve our hits.

To confirm activity as well as benchmark our starting point, we performed dose-response tests on several of our best compounds which identified one sub-micromolar and three single-digit micromolar hits, Table 1. Compound **1** immediately stood out as a molecule of interest, not only as it was the most potent from our screening series, but it also lacked significant activity against BTK and PI3Kδ ((±)-**1**, BTK inh = 24%, PI3Kδ inh = 52% at 100 nM) compared to the other hits. Moreover, (±)-**1** had the largest lipophilic efficiency (LipE = 3.2) among the best hits.

Before embarking on an optimization campaign, we wished to identify the parts of the molecule which were contributing to the inhibitory activity against ATR. Using **1** as the starting point, we identified possible regions of interaction before setting out to prepare the various derivatives, Fig. 3. As the 4-aminopyrazolopyrimidine scaffold was a ubiquitous motif in this series, we speculated that the highlighted region was critical for affinity, likely serving as the kinase hinge binder. However, we could not discount the importance of the azaindolyl group towards ATR affinity at this stage even though no other screening hit contained this substituent. As compounds **1–4** had different *N*-1 substituents, we envisioned that this region was more amenable to changes, but perhaps space-filling would be an important feature.

Compounds **5–8** were designed to examine the importance of the hydrogen-bond donor/acceptor motifs of the 4-aminopyrazolopyrimidine scaffold (**5** and **6**) and of the azaindolyl substituent (**7** and **8**). Compounds **9** and **10** tested the significance of space-filling for groups connected to *N*-1 and *C*-3. The syntheses of compounds **5–10** were prepared from commercially available materials and described in the supplementary material. The ATR inhibition results summarized in Table 2 effectively show a complete loss in ATR binding when either the 4-amino group (**5**) or the nitrogen at position-5 (**6**) are removed. These results demonstrated that this hydrogen-bond donor/acceptor component is in fact a critical element for ATR binding within this molecule class. Replacing the *C*-3 azaindolyl with an indolyl (**7**) resulted in a more modest 7.5-fold loss in ATR IC$_{50}$. Substituting the same azaindolyl with a pyridyl (**8**) resulted in a complete loss of activity against ATR. Interestingly, aminopyridine-containing derivative (**9**) which maintains all the hydrogen-bonding elements of **1** also had diminished activity against ATR albeit with a measurable IC$_{50}$ up to
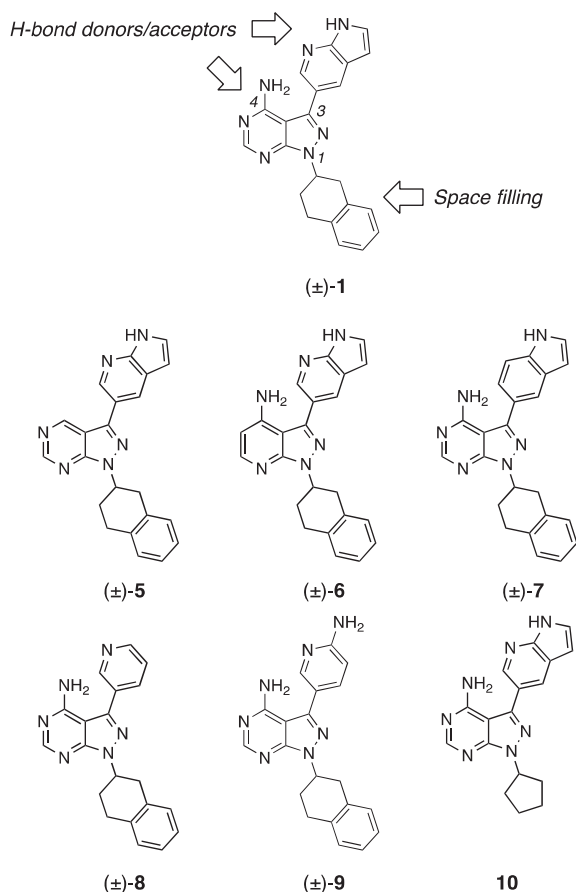
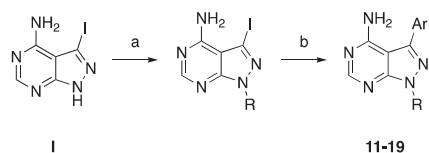Fig. 3. Possible areas of ATR interaction and molecular targets.



**Scheme 1.** Reagents and conditions: (a) R-X, $Cs_2CO_3$, DMF, 70–130 °C, 4 h; (b) Ar-B (OR)$_2$, Pd(PPh$_3$)$_4$, 2 M aqueous Na$_2$CO$_3$, DMF, 100 °C, 16 h.



Fig. 4. Compounds **11**–**19**.

**Table 2**
Results for **1**, **5**–**10**.

| Compound | ATR IC$_{50}$ (µM) | Fold[a] |
|---|---|---|
| (±)-**1** | 0.212 | 1.0 |
| (±)-**5** | >30 | ND[b] |
| (±)-**6** | >30 | ND[b] |
| (±)-**7** | 1.59 | 7.5 |
| (±)-**8** | >30 | ND[b] |
| (±)-**9** | 19.3 | 91 |
| **10** | 1.42 | 6.7 |

[a] Fold = compound IC$_{50}$/(±)-**1** IC$_{50}$.
[b] ND, fold not determined.

30 µM. Together, the results for compounds **7**–**9** suggest that while the hydrogen-bonding elements of the *C*-3 substituent may be beneficial, the space-filling features are critical for activity against ATR. Considering the observed potency of **2** and **3**, it's likely that the para-bromo substituent occupies sufficient space to achieve low-micromolar activity against the protein target. Substituting the tetralinyl group with a cyclopentyl group provided **10** which maintained moderate activity against ATR and only a 6.7-fold loss in activity compared to (±)-**1**. This result supports our previous supposition that the *N*-1 position is more amendable to change than other parts of the molecule.

Having identified key ATR affinity elements within our molecule, we then turned our attention to exploring the effects of different groups at *C*-3. Starting from 4-amino-3-iodopyra-zolopyrimidine, **I**, the desired analogs were prepared by alkylating *N*-1 with tetraline-2-mesylate and then derivatizing with various boronic acids or boronate esters (Scheme 1) to afford compounds **11**–**15**, Fig. 4.
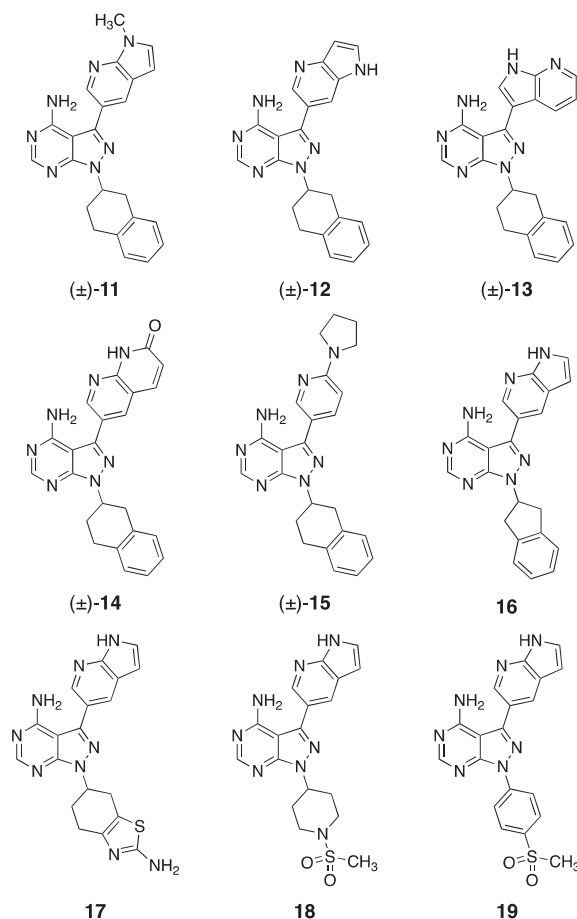
The methylated indole derivative **11** effectively maintained affinity towards ATR and had a slight loss in potency (fold = 2.7) compared to (±)-**1**, Table 3. This further supports our hypothesis that the hydrogen-bonding capacity of the *C*-3 substituent is not an important factor in ATR binding. Somewhat surprisingly, iso-meric indole adduct **12** was attenuated by nearly 10-fold compared to **11** and 22-fold compared to (±)-**1** indicating that stereoelec-tronic effects contributes at least partially towards ATR affinity. Connecting the azaindolyl group through the five-membered ring at the 3′-position (**13**) resulted in a complete loss of ATR activity. It's likely that this new orientation exceeds the limits of the bind-ing pocket, however unfavorable stereoelectronic features cannot be discounted at this time. A similar effect was observed with naphthyridin-2-one analogue **14** which was over 100-fold less potent against ATR compared to (±)-**1**. We also attempted to improve the ATR affinity of **9** by adding another ring to the 2-aminopyridyl group, however the resulting analogue (**15**) was equipotent to **9** and 90-fold less potent relative to (±)-**1**. Taken together, these results begin to describe the binding pocket off of

the *C*-3 position of the pyrazolopyrimidine scaffold, but additional studies such as crystallography would be required to fully define the steric and stereoelectronic features of this region.

Given that our *C*-3 modifications did not improve affinity towards ATR, we chose to maintain the azaindolyl group of **1** when investigating changes at pyrazolopyrimidine *N*-1. Following Scheme 1, we alkylated iodide **I** with a variety of electrophiles and then cross coupled with 7-azaindole-5-boronic acid pinacol ester to provide *N*-1 analogues **16–19**.

Among our first tasks was the resynthesis of (±)-**1** and subsequent resolution of its enantiomers (**1** and **1′**). Although there appears to be a distinction between the two enantiomers of (±)-**1** with respect to ATR affinity, the overall difference is not more than 2-fold (**1** $IC_{50}$ = 0.304 μM vs. **1′** $IC_{50}$ = 0.158 μM), Table 4. Indane-containing analogue **16** eliminates the stereogenic center and slightly alters the trajectory of the *N*-1 substituent. However, this modification does not improve but rather attenuates potency against ATR by approximately 3-fold compared to (±)-**1**. We also employed the *N*-1 group present in **4**. While **17** and **17′** were an improvement relative to **4**, they were essentially equipotent with respect to (±)-**1** (**17** fold = 1.3, **17′** fold = 2.6). Analogue **18** utilizes

a sulfonamide moiety illustrated in a series of ATR inhibitors recently reported by Barsanti *et al.*[22] However, this analogue performed no better than our initial hits providing low-micromolar potency against ATR, (**18**, $IC_{50}$ = 1.32 μM). We also took inspiration from Vertex and employed a phenylsulfonyl group similar to VX970.[25,26] Satisfyingly, **19** was our best ATR inhibitor to date with an $IC_{50}$ = 0.066 μM which represented a 3-fold improvement over screening hit (±)-**1**.

With a double-digit nanomolar ATR inhibitor in hand, we now had a practical analogue with which to obtain a PK-ADME and selectivity profile. To benchmark our development progress, we included clinical candidates VX970 and AZD6738[27] in our ATR and *in vitro* ADME studies alongside **19**. In our hands, VX970 had an $IC_{50}$ = 0.015 μM against ATR and AZD6738 had an $IC_{50}$ = 0.086 μM, Table 5. It's worth noting that reported results for both agents were considerably lower (VX970, lit. $K_i$ < 0.2 nM; AZD6738, lit. $IC_{50}$ = 1 nM) compared to our tests which is likely a result of differences in assay methodologies. Nonetheless, **19** appears to be comparable to both clinical candidates from a biochemical potency standpoint. Moreover, the lipophilic efficiency of **19** was calculated to be 5.8 which is comparable if not an improvement to VX970 and AZD9738. The *in vitro* metabolism assays were performed with either human, mouse or rat liver microsomes, which were supplemented with NADPH to assess oxidative stability (hLM, mLM or rLM). The results for all three compounds demonstrate reasonable oxidative stability across the species tested.

Compound **19** was tested for off-target activity in a panel of 394 kinases at 1 and 10 μM. At 1 μM, **19** inhibited 23 proteins >70% whereas at 10 μM, 76 proteins were inhibited >70%, Fig. 5. Under both conditions, **19** more greatly inhibited ATR (inh = 96% and 106%, 1 μM and 10 μM, respectively) and breast tumor kinase (BRK, inh = 102%, 1 μM and 10 uM) than any others tested. Notable kinase hits >70% at 1 μM include B-Raf (WT and V599E), DDR1, cKit (D816H and V560G) and FMS, Table 6. As the lead compound was derived from a BTK/PI3Kδ dual inhibitor library, we were pleased to observe that **19** only inhibited BTK to 25% and PI3Kδ to 42% at 1 μM. Regarding kinases relevant to DNA damage repair, **19** appears selective for ATR over both ATM (inh = 28% at 1 μM) and DNA-PK (inh = 59% at 1 μM). Overall, **19** appears to be relatively selective with most activity related to the tyrosine kinase family.

Lastly, we evaluated the *in vivo* properties of **19** by conducting pharmacokinetic (PK) studies in mice. Compound **19** was dosed as a solution at 2 mg/kg IV and 10 mg/kg PO. The results are summarized in Table 7. Compound **19** had good clearance in mice, but had poor oral bioavailability indicating improvements in adsorption might be beneficial for further development candidates.

**Table 3**
Results for **11–15**.

| Compound | ATR $IC_{50}$ (μM) | Fold[a] |
|---|---|---|
| (±)-**11** | 0.580 | 2.7 |
| (±)-**12** | 4.62 | 22 |
| (±)-**13** | >30 | ND[b] |
| (±)-**14** | 22.4 | 106 |
| (±)-**15** | 19.1 | 90 |

[a] Fold = compound $IC_{50}$/(±)-**1** $IC_{50}$.
[b] ND, fold not determined.

**Table 4**
Results for **1**, **17–20**.

| Compound | ATR $IC_{50}$ (μM) | Fold[a] |
|---|---|---|
| 1 | 0.304 | 1.4 |
| 1′ | 0.158 | 0.75 |
| 16 | 0.654 | 3.1 |
| 17 | 0.269 | 1.3 |
| 17′ | 0.547 | 2.6 |
| 18 | 1.32 | 6.2 |
| 19 | 0.066 | 0.31 |

[a] Fold = compound $IC_{50}$/(±)-**1** $IC_{50}$.

**Table 5**
ATR $IC_{50}$'s (μM) and *in vitro* ADME for **19**, VX970 and AZD6738.
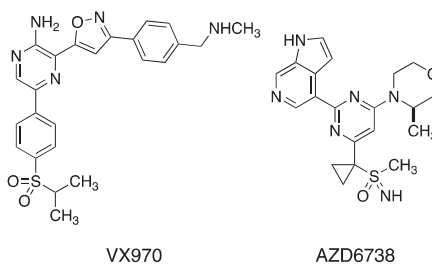


VX970          AZD6738

| Cmpd | ATR $IC_{50}$ (μM) | LipE | hLM[a] | mLM[a] | rLM[a] |
|---|---|---|---|---|---|
| 19 | 0.066 | 5.8 | 83 | 79 | 63 |
| VX970 | 0.015 | 4.7 | 71 | 77 | 80 |
| AZD6738 | 0.086 | 5.2 | 84 | 68 | 93 |

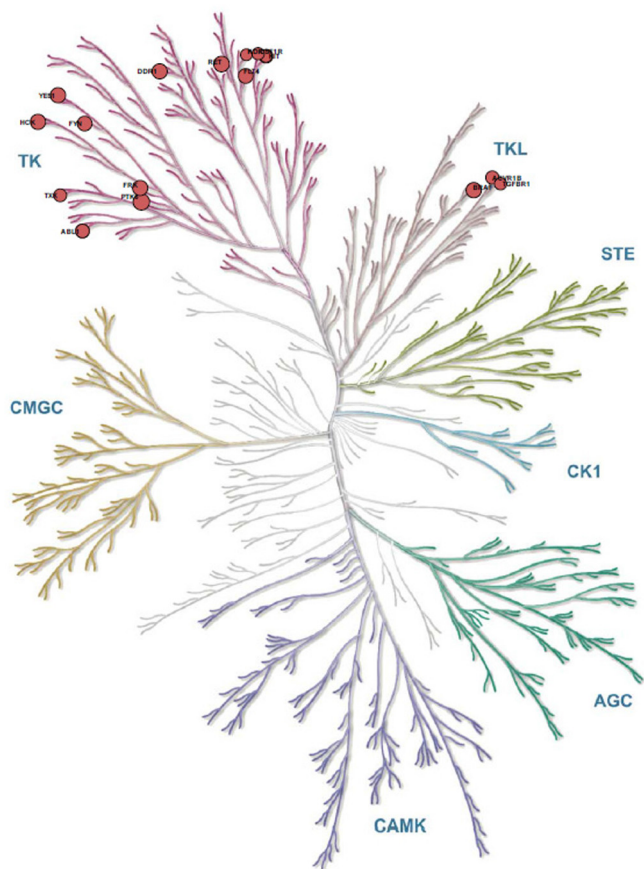[a] Percent parent remaining (%R) after 30 min.

**Fig. 5.** Kinase map of **19** depicting hits > 70% inhibition at 1 μM of 394 kinases tested; atypical protein kinases such as ATR, ATM, mTOR and PRKDC are not listed. See Supplemental Information for full list of kinase activity.

**Table 6**
Selected kinase panel results at 1 μM.

| Kinase | Inh (%) | Kinase | Inh (%) |
|---|---|---|---|
| ATR(h) | 96 | cKit(V560G)(h) | 76 |
| BRK(h) | 102 | FMS | 76 |
| B-Raf(V599E)(h) | 93 | TGFβR1 | 76 |
| DDR1(h) | 92 | DNA-PK(h) | 59 |
| B-Raf(h) | 89 | PI3 Kδ(h) | 42 |
| cKit(D816H)(h) | 85 | ATM(h) | 28 |
| ALK4(h) | 80 | BTK(h) | 25 |

**Table 7**
*In vivo* mouse pharmacokinetic properties[a] of **19**.

| CL (L/h/kg) | $V_z$ (L/kg) | $AUC_{PO}$ (μM•h) | PO $t_{1/2}$ (h) | F (%) |
|---|---|---|---|---|
| 1.33 | 2.15 | 0.212 | 2.28 | 2.83 |

[a] WinNonlin noncompartmental analysis.

Compound **1** was identified as a hit from an ATR biochemical screen of a BTK/PI3Kδ dual inhibitor library. Systematic modifications of the scaffold helped to define the binding mode, particularly the importance of the 4-amino group and the 5-position nitrogen. Variations to the *N*-1 and *C*-3 substituents provided additional information, however more detailed studies are required to fully understand the binding pocket. Further modifications led to the discovery of **19**, a novel pyrazolopyrimidine-containing analogue that: (1) has an ATR $IC_{50}$ = 66 nM; (2) is selective for ATR over ATM and DNA-PK; (3) has acceptable mouse PK properties; and (4) represents a candidate for further cellular and *in vivo* profiling including proof-of-concept (PoC) studies.

## Supplementary material

Supplementary data associated with this article can be found, in the online version, at http://dx.doi.org/10.1016/j.bmcl.2017.01.045.

## References

1. Jackson SP, Bartek J. *Nature*. 2009;461:1071–1078.
2. Mazouzi A, Velimezi G, Loizou JI. *Exp Cell Res*. 2014;329:85–93.
3. Kaelin WG. *Nat Rev Cancer*. 2005;5:689–698.
4. Liang Y, Lin S-Y, Brunicardi FC, Goss J, Li K. *World J Surg*. 2008;33:661–666.
5. Fang B. *J Med Chem*. 2014;57:7859–7873.
6. O'Connor M. *J Mol Cell*. 2015;60:547–560.
7. Kim G, Ison G, McKee AE, et al. *Clin Cancer Res*. 2015;21:4257–4261.
8. Plummer R. *Clin Oncol (R Coll Radiol)*. 2014;26:250–256.
9. Rabenau K, Hofstatter E. *Clin Therap*. 2016;38:1577–1588.
10. Wang Y-Q, Wang P-Y, Wang Y-T, Yang F-F, Zhang A, Miao Z-H. *J Med Chem*. 2016;59:9575–9598.
11. Wagner JM, Kaufmann SH. *Pharmaceuticals*. 2010;3:1311–1334.
12. Fokas E, Prevo R, Hammond EM, Brunner TB, McKenna WG, Muschel RJ. *J Cancer Treatment Rev*. 2014;40:109–117.
13. Foote KM, Lau A, Nissink JW. *Fut Med Chem*. 2015;7:873–891.
14. Hoekstra MF. *Curr Opin Genet Develop*. 1997;7:170–175.
15. Kavanaugh G, Ye F, Mohni KN, Luzwick JW, Glick G, Cortez D. *DNA Repair*. 2015;35:55–62.
16. Prevo R, Fokas E, Reaper PM, et al. *Can Biol Therap*. 2014;13:1072–1081.
17. Mohni KN, Thompson PS, Luzwick JW, et al. *PLoS One*. 2015;10:e0125482.
18. Pollard J, Reaper P, Peek A, et al. *Can Res*. 2016;76:3711.
19. Krajewska M, Fehrmann RSN, Schoonen PM, et al. *Oncogene*. 2015;34:3474–3481.
20. Charrier J-D, Durrant SJ, Golec JMC, et al. *J Med Chem*. 2011;54:2320–2330.
21. Foote KM, Blades K, Cronin A, et al. *J Med Chem*. 2013;56:2125–2138.
22. Barsanti PA, Aversa RJ, Jin X, et al. *ACS Med Chem Lett*. 2015;6:37–41.
23. Barsanti PA, Pan Y, Lu Y, et al. *ACS Med Chem Lett*. 2015;6:42–46.
24. Pujala B, Agarwal AK, Middya S, et al. *ACS Med Chem Lett*. 2016;ASAP.
25. Fokas E, Prevo R, Pollard JR, et al. *Cell Death Dis*. 2012;3:e441.
26. Hall AB, Newsome D, Wang Y, et al. *Oncotarget*. 2014;5:5674–5685.
27. Vendetti FP, Lau A, Schamus S, Conrads TP, O'Connor MJ, Bakkenist CJ. *Oncotarget*. 2015;6:44289–44305.